

# Aerosol microphysics modules in the framework of the ECHAM5 climate model – intercomparison under stratospheric conditions

H. Kokkola<sup>1,2</sup>, R. Hommel<sup>1,4</sup>, J. Kazil<sup>1</sup>, U. Niemeier<sup>1</sup>, A.-I. Partanen<sup>1,3,5</sup>, J. Feichter<sup>1</sup>, and C. Timmreck<sup>1</sup>

<sup>1</sup>Max Planck Institute for Meteorology, Hamburg, Germany

<sup>2</sup>Finnish Meteorological Institute, Kuopio, Finland

<sup>3</sup>Tampere University of Technology, Tampere, Finland

<sup>4</sup>Centre for Atmospheric Science, Cambridge University, Department of Chemistry, Cambridge, UK

<sup>5</sup>University of Kuopio, Department of Physics, Finland

Received: 26 February 2009 – Published in Geosci. Model Dev. Discuss.: 9 March 2009

Revised: 14 July 2009 – Accepted: 14 July 2009 – Published: 28 July 2009

**Abstract.** In this manuscript, we present an intercomparison of three different aerosol microphysics modules that are implemented in the climate model ECHAM5. The comparison was done between the modal aerosol microphysics module M7, which is currently the default aerosol microphysical core in ECHAM5, and two sectional aerosol microphysics modules SALSA, and SAM2. The detailed aerosol microphysical model MAIA was used as a reference to evaluate the results of the aerosol microphysics modules with respect to sulphate aerosol.

The ability of the modules to describe the development of the aerosol size distribution was tested in a zero dimensional framework. We evaluated the strengths and weaknesses of different approaches under different types of stratospheric conditions. Also, we present an improved method for the time integration in M7 and study how the setup of the modal aerosol modules affects the evolution of the aerosol size distribution.

Intercomparison simulations were carried out with varying SO<sub>2</sub> concentrations from background conditions to extreme values arising from stratospheric injections by large volcanic eruptions. Under background conditions, all microphysics modules were in good agreement describing the shape of the aerosol size distribution, but the scatter between the model results increased with increasing SO<sub>2</sub> concentrations. In particular in the volcanic case the setups of the aerosol modules have to be adapted in order to dependably capture the evolu-

tion of the aerosol size distribution, and to perform in global model simulations.

In summary, this intercomparison serves as a review of the different aerosol microphysics modules which are currently available for the climate model ECHAM5.

## 1 Introduction

While greenhouse gases such as carbon dioxide and methane have been shown to have a large effect on climate by warming the Earth's surface when absorbing the long wave radiation emitted from earth (e.g. Fleming, 1998; Le Treut et al., 2007; Weart, 2003), it has been acknowledged that increased atmospheric concentrations of aerosol particles might drive a significant radiative forcing process of the planet (Twomey, 1974; Seinfeld and Pandis, 1998; IPCC, 2007). The knowledge of the impacts of aerosols on health, atmospheric composition and climate is still incomplete. Even more uncertainties lie in the understanding of direct and indirect effects of aerosols on climate and how these effects are modified by aerosol processing and aerosol composition (Chen and Penner, 2005).

To comprehensively assess the impact of aerosol particles on ozone concentration, cloud formation and radiative forcing, information about the particle size and number density is necessary (e.g. Zhang et al., 2002; Dusek et al., 2006). In global scale atmospheric models, modeling aerosol processes is always a compromise between accuracy and computational efficiency. Thus the descriptions of the aerosol size as well as the chemical composition of aerosol populations have to



Correspondence to: H. Kokkola  
(harri.kokkola@fmi.fi)

be simplified. The aerosol distribution in aerosol modules is described in most cases using the bulk approach (Liao and Seinfeld, 2005; Liu et al., 2005; Reddy et al., 2005; Rasch et al., 2008), modal approach (Ghan et al., 2001; Wilson et al., 2001; Herzog et al., 2004; Vignati et al., 2004; Lauer et al., 2005; Stier et al., 2005), and sectional approach (Weisenstein et al., 1997; Jacobson, 2001; Timmreck, 2001; Rodriguez and Dabdub, 2004; Spracklen et al., 2005; Hommel, 2008; Kokkola et al., 2008). In the bulk approach, only the aerosol mass is prognostic. The particle sizes can then be retrieved assuming e.g. monodisperse or prescribed size distributions. The bulk approach is computationally very efficient, but introduces a large error when calculating strongly size dependent physical effects of aerosols, such as scattering of radiation and cloud activation (e.g. Zhang et al., 2002). While in the mono-disperse approach a particle population is assumed to be of uniform size, both modal and sectional aerosol schemes resolve entire particle spectra and are able to consider more than a single aerosol moment. Several model studies highlight the importance of a simultaneous prognostic treatment of both aerosol mass and number for aerosol-climate process interactions (e.g. Adams and Seinfeld, 2002). Depending on the number of aerosol species treated by the aerosol modules, the modal approach is computationally more efficient than the sectional approach, and the demands of the latter in global climate simulations can easily exceed today's available high performance computing facilities (e.g. Ghan and Schwartz, 2007). Nevertheless, simplifying the aerosol size distribution by the assumption of log-normal modes is a source of uncertainty when the shape of the size distribution is heavily modified by microphysical processes. This can be crucial especially in studies of evolving perturbations of the stratospheric aerosol layer since the mean aerosol life time there can achieve several years, compared to a few days under tropospheric conditions (e.g. WMO/SPARC, 2006).

Under stratospheric background conditions, concentrations of sulphate aerosol precursor gases remain below 1 ppb and the stratospheric background aerosol load is estimated to be  $0.65 \pm 0.2$  Tg (WMO/SPARC, 2006). In case of large volcanic eruptions, the stratospheric sulphate mass increased for a short time period approximately one to two orders of magnitude. After the Pinatubo eruption, the maximum aerosol load has been estimated to be 30 Tg (McCormick et al., 1995). Not only the aerosol mass but also the particle size increased from a typical background effective radius of  $0.17 \pm 0.07$   $\mu\text{m}$  to a peak value of  $0.5$   $\mu\text{m}$  during the 1991 Pinatubo eruption.

The size distribution of the stratospheric aerosol population has a strong influence on climate, which has become of increasing scientific interest in the light of geoengineering the climate using human-induced sulphate aerosol (e.g. Crutzen, 2006; Rasch et al., 2008). Hence it is important to assess the abilities of different microphysical approaches to simulate the temporal development of particle size distri-

butions under evolving atmospheric conditions. Comparison of stratospheric aerosol models on a global scale have been carried out recently in the frame of the SPARC Aerosol Assessment (WMO/SPARC, 2006) and the Global Model Initiative intercomparison (Weisenstein et al., 2007) pointing to a range of uncertainties in the model predictions in particular transport rates.

In the following we will focus in the first step on model differences not influenced by any transport or removal processes investigating initial changes in the sulphate aerosol distribution after an enhancement of the stratospheric  $\text{SO}_2$  loading encompassing small and large (Mt. Pinatubo size) volcanic eruptions and geoengineering case studies. For our studies we will use boxmodel versions of aerosol microphysical models implemented in the global climate model ECHAM5 (Roeckner et al., 2003) which will be tested against a highly resolved particle spectrum model MAIA (Kazil et al., 2007). Special emphasis will be placed on the simulation of the effective radius ( $R_{\text{eff}}$ ), which characterizes aerosol populations independent of the shape of their distribution and turned out to be more sensitive to model formulation than mass or surface area density (Weisenstein et al., 2007).

The size distribution of aerosol populations has a strong influence on climate, as larger particles scatter less visible light than smaller particles and, in the case of non-sulphate or mixed phase aerosol, absorb more efficiently in the near- and far-infrared. It is therefore important to assess the abilities of different microphysical approaches to simulate the temporal development of particle size distributions under evolving atmospheric conditions (volcanoes, geoengineering). In the following, we will focus on initial changes in the stratospheric sulphate aerosol distribution after a volcanic eruption encompassing small and large (Mt. Pinatubo size)  $\text{SO}_2$  emissions.

In Sect. 2, the principal features of the aerosol microphysics modules participating in this intercomparison are introduced. A detailed description of the improved time integration scheme for M7 is given in Sect. 3, followed by an illustration of its performance compared with the variable-coefficient ordinary differential equation solver (VODE). In Sect. 4, the experimental conditions are described. In Sect. 5, different treatments of resolving the aerosol spectra in M7 are compared, and the simulated number distributions of all participating aerosol modules under stratospheric conditions, varying the initial  $\text{SO}_2$  concentration from typical background to extreme volcanic conditions are investigated. The effective radii of the aerosol size distributions from the different simulations and aerosol modules are discussed. A summary is given in Sect. 6.

## 2 Aerosol microphysics modules

In this intercomparison, we compare four different aerosol microphysics modules MAIA, SAM2, SALSA, and M7. Of

**Table 1.** Major characteristics of M7, SALSA, SAM2, and MAIA.

	M7	SALSA	SAM2	MAIA
Method for describing the size distribution	modal	sectional, moving center and fixed center for three largest size sections	sectional, fixed center	hybrid kinetic-sectional, fixed center, first order approximation of size distribution inside geometric size sections
Number of modes or size sections	7	20 (10 in size space)	44	21 kinetic, 99 geometric
Chemical species treated	sulphate, organic carbon, mineral dust, sea salt	sulphate, organic carbon, mineral dust, sea salt	sulphate	sulphate
References	Vignati et al. (2004), Stier et al. (2005)	Kokkola et al. (2008)	Hommel (2008), Timmreck and Graf, 2000	Lovejoy et al. (2004), Kazil et al. (2007)

these, MAIA and SAM2 treat sulphate as the sole aerosol chemical component while SALSA and M7 include also organic compounds, sea salt, black carbon, and mineral dust. The modules describe the processing of aerosol size distribution through the following microphysical processes:

- New particle formation by nucleation.
- Condensation of gas phase compounds to the particle phase.
- Coagulation of the aerosol particles.
- Thermodynamical equilibrium between liquid water and water vapour.

Table 1 summarizes the major features of the aerosol microphysics modules. Three modules of this intercomparison, M7, SALSA, and SAM2 have been designed to be used in large scale climate models and have all been implemented in the climate model ECHAM5. Since these microphysics modules have been designed for large scale models, they parameterize aerosol microphysical processes and use assumptions to resolve the aerosol size distribution. Binary homogeneous nucleation of sulphate aerosols is treated identically in all the three modules using nucleation scheme by Vehkamäki et al. (2002) extending it for high concentrations of sulphate using collision rate as nucleation rate (H. Vehkamäki, personal communication, 2008). For other microphysical processes the treatment varies between the modules. To evaluate the results of these modules, the aerosol model MAIA was considered as a reference since it has a highly resolved particle size spectrum and it is based on advanced numerical, thermodynamical and kinetic approaches compared to parameteri-

zations which are currently used in aerosol modules suitable for global climate simulations.

Since all modules in this intercomparison include sulphate, we chose it to be the sole aerosol compound treated in the simulations. This way we can ensure identical conditions for all the modules and that the results of different modules are comparable and the differences in results are only due to methods used to calculate the microphysical processes.

This idealized experimental setup, of course, does not represent realistic stratospheric conditions. In particular during the first days of an eruption, insoluble compounds like volcanic ash are major constituents of volcanic plumes (see Niemeier et al., 2009). However, fine ash particles are large compared to aerosols and sediment out very quickly so that they are not relevant for long term climate effects (Schneider et al., 1998). In addition, here we focus on the ability of aerosol modules to simulate the climate effect of an enhanced stratospheric sulphate load, either due to volcanic eruptions or due to geoengineering efforts.

In our model setup we neglect the non-microphysical processes such as gravitational settling. The gravitational settling removes coarse particles ( $> 1 \mu\text{m}$ ) when the simulation time extends over several days and neglecting it can cause an overestimation of particle numbers of the coarse particles. On the other hand, in the atmosphere, the sedimented particles will to some extent be replaced by coarse particles from the upper levels. More importantly, as can be seen later in Sect. 5, this approach shows how the modules perform in “extreme conditions” and reveals weaknesses in the methods used by these modules.

Even though the microphysics modules all solve the same microphysical processes, the methods used in the modules

vary significantly. Following is a brief description of formulation of the microphysics modules including improvements introduced in the modules in this study.

## 2.1 MAIA

The reference model in this study is the detailed aerosol model MAIA (Model of Aerosols and Ions in the Atmosphere) (Lovejoy et al., 2004; Kazil et al., 2007). MAIA simulates microphysical processes of neutral and charged (negative)  $\text{H}_2\text{SO}_4/\text{H}_2\text{O}$  aerosol particles. The aerosol size distribution is represented with a hybrid kinetic-sectional scheme: In the kinetic part, the model solves the differential equations for the concentrations of each aerosol particle containing up to 21  $\text{H}_2\text{SO}_4$  molecules. For particles with a larger  $\text{H}_2\text{SO}_4$  content, the model uses geometric size sections: The aerosol size distribution is divided into size ranges; particles in neighbouring size ranges differ by a constant factor in their  $\text{H}_2\text{SO}_4$  content. The model solves the differential equations for the concentrations of aerosol particles within each size range. The size distribution within these geometric size sections is resolved with linear functions. This approach suppresses numerical diffusion better than a doubling of the number of size sections at a negligible computational expense. The system of differential equations for the particle concentrations is integrated with the VODE solver (Brown et al., 1989).

MAIA describes nucleation of sulphate aerosol and growth of the freshly nucleated particles using laboratory thermochemical data for the uptake/loss of gas phase  $\text{H}_2\text{SO}_4$  and  $\text{H}_2\text{O}$  by small neutral and charged molecular clusters (Curtius et al., 2001; Lovejoy and Curtius, 2001; Froyd and Lovejoy, 2003a,b; Hanson and Lovejoy, 2006). The thermochemical data for  $\text{H}_2\text{SO}_4/\text{H}_2\text{O}$  uptake and loss by large aerosol particles derive from the liquid drop model and  $\text{H}_2\text{SO}_4$  and  $\text{H}_2\text{O}$  vapour pressures over bulk solutions, calculated with a computer code (S. L. Clegg, personal communication, 2007) that is based on Giauque et al. (1960); Clegg et al. (1994). The thermochemical data for uptake/loss of gas phase  $\text{H}_2\text{SO}_4$  and  $\text{H}_2\text{O}$  by intermediate sized particles are a smooth interpolation of the data for the small and large particles (see Lovejoy et al., 2004; Kazil et al., 2007). The rate coefficients for sulphuric acid uptake and loss by the aerosol particles, for the coagulation of the aerosol particles, and for the recombination of the negatively charged aerosol with cations are calculated with the Fuchs formula for Brownian coagulation (Fuchs, 1964) and averaged over the equilibrium  $\text{H}_2\text{O}$  content probability distribution of the aerosol. This simplification holds well at the  $\text{SO}_2$  concentrations in the stratospheric conditions used in this work down to a relative humidity of 1%, where water vapour is still more abundant by several orders of magnitude than gas phase sulphuric acid in the MAIA runs, so that the aerosol particles have ample time to equilibrate with respect to water uptake/loss before colliding with a  $\text{H}_2\text{SO}_4$  molecule.

## 2.2 M7

M7 (Vignati et al., 2004) is the microphysical core of aerosol module HAM (Stier et al., 2005) of ECHAM5. The aerosol microphysics module M7 describes the aerosol size-distribution by 7 log-normal modes, predicting the mode size, mixing state, and composition. In the default setup of M7, the modes are assumed to have a fixed geometric standard deviation  $\sigma_g$  of 2.0 for coarse modes and 1.59 for finer modes, so the size distribution can be described by mode radius  $R_p$ , number concentration and composition and thus less variables are needed to describe the particle size interval compared to a sectional model. This makes M7 computationally very efficient.

The aerosol population is divided into two types of particles: mixed, or water-soluble particles, and insoluble particles. Soluble aerosols are assumed to exist in nucleation mode ( $R_p < 0.005 \mu\text{m}$ ), Aitken mode ( $0.005 \mu\text{m} < R_p < 0.05 \mu\text{m}$ ), accumulation mode ( $0.05 \mu\text{m} < R_p < 0.5 \mu\text{m}$ ), and coarse mode ( $R_p > 0.5 \mu\text{m}$ ), while insoluble aerosols are assumed to exist in Aitken, accumulation, and coarse mode. However, since in this intercomparison, only sulphate is treated, the insoluble modes are not used in the simulations.

Previously, M7 has integrated the differential equation for the aerosol compounds using a computationally efficient operator splitting scheme (Vignati et al., 2004). However, this approach may result in numerical errors when time steps typical for global scale models are used. An improved time integration scheme for M7 is described in Sect. 3.

## 2.3 SALSALSA

SALSALSA follows the formulation of M7 using a sectional approach as opposed to the modal approach of M7. The size sections are divided in three subranges with a different degree of external mixing, width of the size sections, and number of chemical compounds. Particle diameters in the different subranges and their chemical composition are defined as follows: Subrange 1: particles with diameter  $D_p < 0.05 \mu\text{m}$ , Subrange 2:  $0.050 \mu\text{m} \leq D_p < 0.73 \mu\text{m}$ , and Subrange 3:  $D_p \geq 0.73 \mu\text{m}$ .

- Subrange 1: Three internally mixed size sections consisting of sulphate and organic carbon. Sizes are calculated using the moving center method (Jacobson, 2005).
- Subrange 2: Four sections in the size space. Each size section includes two parallel size bins, one for potential CCN particles and one for cloud inactive particles. Compounds that are treated in this subrange are sea salt, sulphate, organic carbon, black carbon and mineral dust.
- Subrange 3: three sections in the size space. Each size section includes three parallel size bins, one for completely soluble particles, one for cloud active insoluble

particles, and one for cloud inactive insoluble particles. Particle sizes in the subrange 3 are calculated using the fixed center method, since the sizes of these particles are not assumed to be sensitive to microphysical processing in most atmospheric conditions.

Since in this intercomparison, sulphate is considered as the sole chemical component in the aerosol particles, the insoluble size sections are not used in this intercomparison, reducing the number of size sections to 10. When insoluble size sections are used the number of size sections in SALSA is 20.

For nucleation, SALSA applies the parameterization by Kerminen and Kulmala (2002), which determines the formation rate of 3 nm particles from the nucleation rate given by the Vehkamäki et al. (2002) scheme. Condensation of gas phase compounds onto the particles is calculated concurrently with nucleation using the analytical predictor of nucleation and condensation method (Jacobson, 2005). Coagulation is calculated using a semi-implicit method (Jacobson, 1994).

For a more detailed description of the treatment of aerosol compounds, methods for microphysical processes, and the division of size sections in SALSA, see Kokkola et al. (2008).

## 2.4 SAM2

SAM2 is a one moment aerosol scheme treating the aerosol mass in each bin prognostically. The scheme follows the fixed sectional approach (Gelbard et al., 1980) to resolve an aerosol distribution from  $1 \times 10^{-3} \mu\text{m}$  to  $20.64 \mu\text{m}$  in radius. 44 logarithmically spaced size bins are determined by mass doubling.

Unlike M7 and SALSA, which assume zero saturation vapour pressure of  $\text{H}_2\text{SO}_4$  at the particle surface, SAM2 is able to treat the mass transfer of sulphuric acid vapour reversely without further parameterizations for evaporating particles. Considering that the latter process is of relevance for global aerosol-climate models designated for investigations of volcanic effects on stratospheric aerosol, since evaporation determines the vertical limitation of the global dispersion of liquid aerosol particles in regions where the stratosphere is locally subsaturated with respect to their vapour concentrations (Hamill et al., 1977). In SAM2 the change in the aerosol size distribution due to reversible gas-to-particle partitioning of  $\text{H}_2\text{SO}_4$  is treated as an advective type process that allows particles to grow and shrink virtually in size space. Here a one-dimensional hybrid exponential-upwind advection scheme (Spalding, 1972; Chlond, 1994; Timmreck and Graf, 2000) ensures the preservation of the particle number concentration under conditions of the “whole atmosphere”. This is of special interest when an aerosol distribution is characterized by rapid changes, which can be caused by e.g. ultrafine aerosols nucleating from the gas phase.

Brownian coagulation is considered following a semi-implicit mass conserving formulation by (Timmreck and Graf, 2000). As opposed to the time integration scheme of SALSA and the new time integration scheme of M7, the time integration of individual microphysical processes in SAM2 is processed sequentially. A complete description of the parameterizations implemented in SAM2 and its overall performance in the context of a global aerosol-climate model resolving the troposphere and the stratosphere up to  $\sim 80 \text{ km}$  can be found in Hommel (2008).

## 3 New time integration scheme of $\text{H}_2\text{SO}_4$ processes in M7

A new method for the integration of the time evolution equation

$$\frac{d[\text{H}_2\text{SO}_4]}{dt} = P - C \cdot [\text{H}_2\text{SO}_4] - R([\text{H}_2\text{SO}_4]) \quad (1)$$

for the concentration of gas phase sulphuric acid has been implemented in the M7 aerosol microphysics module.  $P$  denotes the production rate of gas phase  $\text{H}_2\text{SO}_4$ ,  $C$  its loss rate due to condensation onto aerosol particles,  $R([\text{H}_2\text{SO}_4])$  the removal rate of gas phase sulphuric acid due to aerosol nucleation, and  $t$  the time.  $P$  and  $C$  depend on gas and aqueous phase chemistry and aerosol microphysics, and are determined in separate time integration (operator splitting) procedures before or after the integration of Eq. (1). They are considered constant for the integration of Eq. (1) over one time step.

In the Euler backward scheme, Eq. (1) is discretized as

$$\frac{[\text{H}_2\text{SO}_4]_{t+\Delta t} - [\text{H}_2\text{SO}_4]_t}{\Delta t} = P - C \cdot [\text{H}_2\text{SO}_4]_{t+\Delta t} - R([\text{H}_2\text{SO}_4]_{t+\Delta t}) \quad (2)$$

which can be rewritten to

$$[\text{H}_2\text{SO}_4]_{t+\Delta t} = \frac{[\text{H}_2\text{SO}_4]_t + \Delta t P - \Delta t R([\text{H}_2\text{SO}_4]_{t+\Delta t})}{1 + \Delta t C}. \quad (3)$$

This equation is then solved for  $[\text{H}_2\text{SO}_4]_{t+\Delta t}$ , typically iteratively. However, the iteration and a repeated evaluation of the removal rate  $R$  until a satisfactory degree of convergence is achieved may not to be computationally affordable. A common approach is then to abort the iteration after all processes have been calculated once. This can be realized with operator splitting between production/condensation and nucleation: When the iteration is initialized as

$$\begin{aligned} [\text{H}_2\text{SO}_4]_{t+\Delta t}^0 &= \frac{[\text{H}_2\text{SO}_4]_t + \Delta t P}{1 + \Delta t C} \\ [\text{H}_2\text{SO}_4]_{t+\Delta t}^1 &= \frac{[\text{H}_2\text{SO}_4]_t + \Delta t P - \Delta t R([\text{H}_2\text{SO}_4]_{t+\Delta t}^0)}{1 + \Delta t C} \\ &\vdots \end{aligned} \quad (4)$$

**Table 2.** Ambient parameters and the initial values for the the production rate of gas phase sulphuric acid, the pre-existing aerosol size distribution, and sulphuric acid gas phase concentration for the evaluation of the new time integration scheme for three different test cases.

	case 1	case 2	case 3
Temperature (K)	255	225	285
RH (%)	80	50	90
production rate ( $\text{cm}^{-3}\text{s}^{-1}$ )	100000	10000	50000
condensation sink ( $\text{s}^{-1}$ )	0.001	0.0001	0.01
Initial $[\text{H}_2\text{SO}_4]$ ( $\text{cm}^{-3}$ )	$1 \times 10^6$	$7.5 \times 10^7$	$1 \times 10^8$

then the first two steps can be interpreted as

$$[\text{H}_2\text{SO}_4]_{t+\Delta t}^{PC} = \frac{[\text{H}_2\text{SO}_4]_t + \Delta t P}{1 + \Delta t C} \quad (5)$$

$$[\text{H}_2\text{SO}_4]_{t+\Delta t}^{PCN} = [\text{H}_2\text{SO}_4]_{t+\Delta t}^{PC} - \frac{\Delta t R([\text{H}_2\text{SO}_4]_{t+\Delta t}^{PC})}{1 + \Delta t C} \quad (6)$$

which corresponds to calculating the concentration of gas phase  $\text{H}_2\text{SO}_4$  after production and condensation ( $PC$ ) and then after nucleation ( $PCN$ ). However,  $[\text{H}_2\text{SO}_4]_{t+\Delta t}^{PC}$  in Eq. (5) can be computed exactly by exploiting the fact that if nucleation is neglected, Eq. (1) has an analytical solution:

$$[\text{H}_2\text{SO}_4](t) = \left( [\text{H}_2\text{SO}_4](t_0) - \frac{P}{C} \right) \cdot e^{-C(t-t_0)} + \frac{P}{C}. \quad (7)$$

The new integration method therefore reads

$$[\text{H}_2\text{SO}_4]_{t+\Delta t}^{PC} = \left( [\text{H}_2\text{SO}_4]_t - \frac{P}{C} \right) \cdot e^{-C\Delta t} + \frac{P}{C} \quad (8)$$

$$[\text{H}_2\text{SO}_4]_{t+\Delta t}^{PCN} = [\text{H}_2\text{SO}_4]_{t+\Delta t}^{PC} - \frac{\Delta t R([\text{H}_2\text{SO}_4]_{t+\Delta t}^{PC})}{1 + \Delta t C}$$

Unlike the Euler backward scheme and the original M7 time integration method, the new time integration has the advantage to converge towards the exact solution of Eq. (1) for all time step lengths with decreasing nucleation ( $R \rightarrow 0$ ). As in the original M7 time integration, a safeguard is implemented which prevents the gas phase sulphuric acid concentration from becoming negative: When the removal due to nucleation in the course of a time step would exceed the initially available and newly produced gas phase sulphuric acid, all of it is converted to newly formed particles, and its concentration is set to zero.

### 3.1 Testing new time integration scheme

In order to illustrate the performance of the new time integration scheme we compare it with the Euler backward scheme, the original M7 time integration method, and the VODE

solver (Brown et al., 1989) which uses the variable coefficient Adams-Moulton method for non-stiff ordinary differential equations and time step lengths based on a desired relative error tolerance.

Three different cases were considered, with ambient conditions chosen so that  $\text{H}_2\text{SO}_4$  decreases, is kept constant, or increases, without focus on particular geophysical conditions. The conditions for the three cases are given in Table 2. The same pressure (1013.25 hPa), ion pair production rate ( $4 \text{ cm}^{-3}\text{s}^{-1}$ ), diameter of the preexisting aerosol particles ( $0.165 \mu\text{m}$ ), and mass density of the preexisting aerosol particles ( $2 \text{ g cm}^{-3}$ ) was used in all three cases. Nucleation rates and the resulting removal rates of gas phase sulphuric acid were calculated with the method of Kazil and Lovejoy (2007).

Figure 1 shows the gas phase sulphuric acid concentration after one time step, as a function of the time step length, calculated with the new time integration method, the Euler backward scheme, and the original M7 method. As a reference, the gas phase sulphuric acid concentration calculated with the VODE solver is given, which divides the time step into shorter integration steps, based on a desired relative error tolerance ( $10^{-9}$  in this comparison).

In cases 1 and 3 the new time integration method performs as well as VODE and better than the Euler backward scheme. In case 2 the new time integration method and the Euler backward scheme produce very similar results (overlapping curves), both underestimating the sulphuric acid concentration obtained with the VODE solver. The systematic bias is increasing with increasing time step length. In contrast, the original M7 method significantly underestimates sulphuric acid gas phase concentrations in all three cases, and predicts a total removal of the available sulphuric acid in the gas phase at longer time step lengths in the cases 1 and 3. The underestimation of the gas phase concentrations for shorter time step lengths arises from an overestimation of condensation by this scheme. The zero values in cases 1 and 3 for longer time steps result from an overestimation of the loss of sulphuric acid via nucleation, which exceeds the available gas phase sulphuric acid, and which is entirely converted to new particles. A complete conversion of the available gas phase sulphuric acid to new particles can also result with the new time integration method and the Euler backward scheme, but requires higher nucleation rates or longer time steps compared with the original M7 method.

The new time integration method outperforms both the original M7 method and the Euler backward scheme for the solution of the gas phase sulphuric acid time evolution equation with concurrent nucleation and condensation. In the following simulations, we have used this new time integration method.

#### 4 Experimental setup

The ability of the microphysics modules to describe the processing of the sulphate aerosol size distribution was investigated by calculating the evolution of the size distribution over a 10 day period assuming typical conditions of the mid-latitude stratosphere at 30 hPa ambient pressure and 214.8 K temperature. Initial stratospheric sulphate size distribution was assumed to be unimodal with  $0.234 \mu\text{m}$  geometric mean diameter, 1.59 geometric standard deviation, and a total number concentration of  $3 \text{ cm}^{-3}$ . The simulations were carried out in a zero dimensional framework in order to distinguish the differences between the modules in the treatment of microphysical processes.

The evolution of the size distribution was affected by varying the initial  $\text{SO}_2$  concentration which modifies the size distribution through oxidation to  $\text{H}_2\text{SO}_4$  and subsequent gas-to-particle partitioning processes. We assume that gaseous  $\text{H}_2\text{SO}_4$  is exclusively formed from the oxidation of  $\text{SO}_2$  by the hydroxyl radical OH. The concentration of the latter is prescribed by an abstracted diurnal cycle with a daytime concentration of  $1 \times 10^6 \text{ cm}^{-3}$  between 06:00 and 18:00. This value was derived from a time slice experiment conducted with the chemistry-climate model MAECHAM4-CHEM (Timmreck et al., 2003). The initial  $\text{SO}_2$  mixing ratio was varied between a typical background value of  $1.5 \times 10^{-11} \text{ kg/kg}$  ( $\sim 10 \text{ pptv}$ ; WMO/SPARC, 2006) and  $3.9 \times 10^{-4} \text{ kg/kg}$  for the assumed volcanic case and two intermediate mixing ratios of  $3.9 \times 10^{-8} \text{ kg/kg}$  and  $3.9 \times 10^{-6} \text{ kg/kg}$ . The extreme case mixing ratio of  $3.9 \times 10^{-4} \text{ kg/kg}$  was derived from a MAECHAM5 simulation of the June 1991 Mt. Pinatubo eruption (Niemeier et al., 2009). In this 3-D simulation 17 Mt of  $\text{SO}_2$  was initialized according to satellite observations after the Pinatubo eruption (Read et al., 1993).

The sensitivity studies presented in the following were conducted using integration time step length of  $\Delta t = 1 \text{ s}$ , 60 s, and 900 s. The latter corresponds to the default time step of ECHAM5 using the spectral truncation T42.

In M7, the standard deviation  $\sigma_g$  of the individual modes is fixed, so the choice of the value for  $\sigma_g$  affects the module's ability to describe the development of the size distribution especially in conditions where the shape of the size distribution is heavily modified, for example when high concentrations of sulphuric acid vapour yield high mass transfer rates into the particle phase. The role of the coarse mode in M7 is to describe primary sea salt and dust particles which are mainly present in the troposphere. Sulphate aerosol can be accurately described with three modes, as shown in the M3 module (Wilson and Raes, 1996; Wilson et al., 2001), a predecessor module of M7. Therefore we tested two different mode setups in M7, the default mode setup and a second setup in which the coarse mode was neglected.

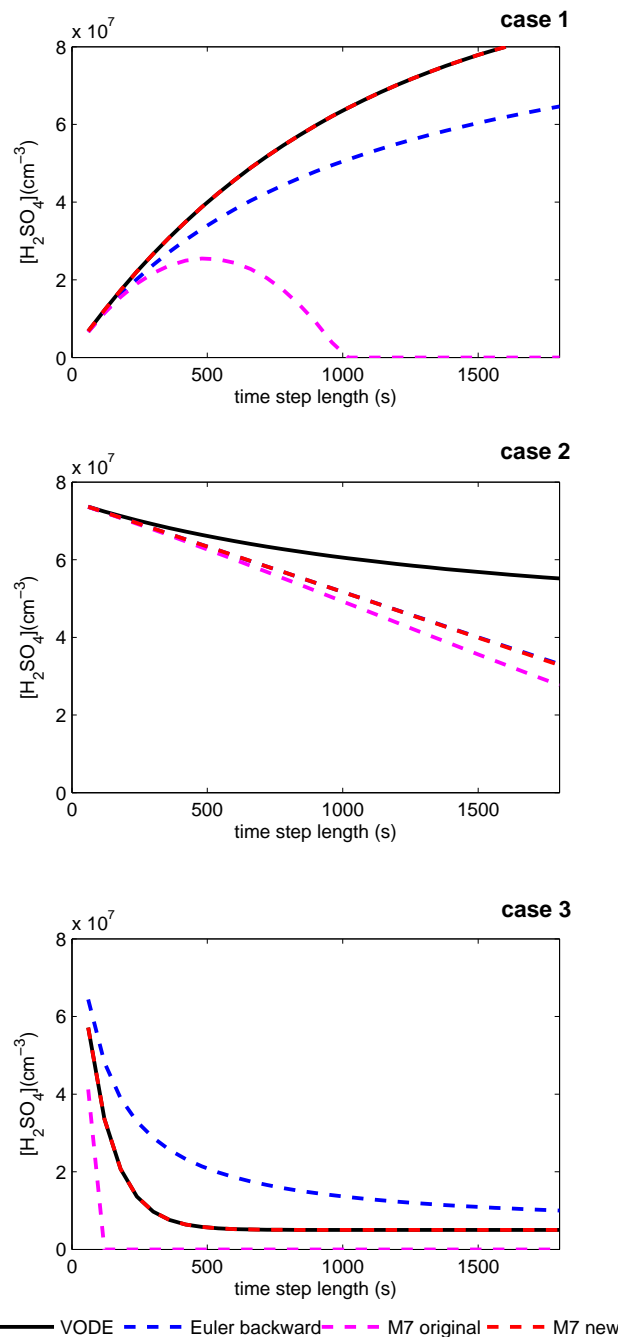


**Fig. 1.** Gas phase concentration of sulphuric acid after one time step, calculated with the Euler backward scheme, the original M7 operator splitting method, and the new time integration method. As a reference, the gas phase sulphuric acid concentration calculated with the VODE solver is given. In this case, the abscissa denotes the integration time, which is divided into shorter time steps by VODE according to a desired relative error tolerance. Parameters for the three cases are given in Table 2.

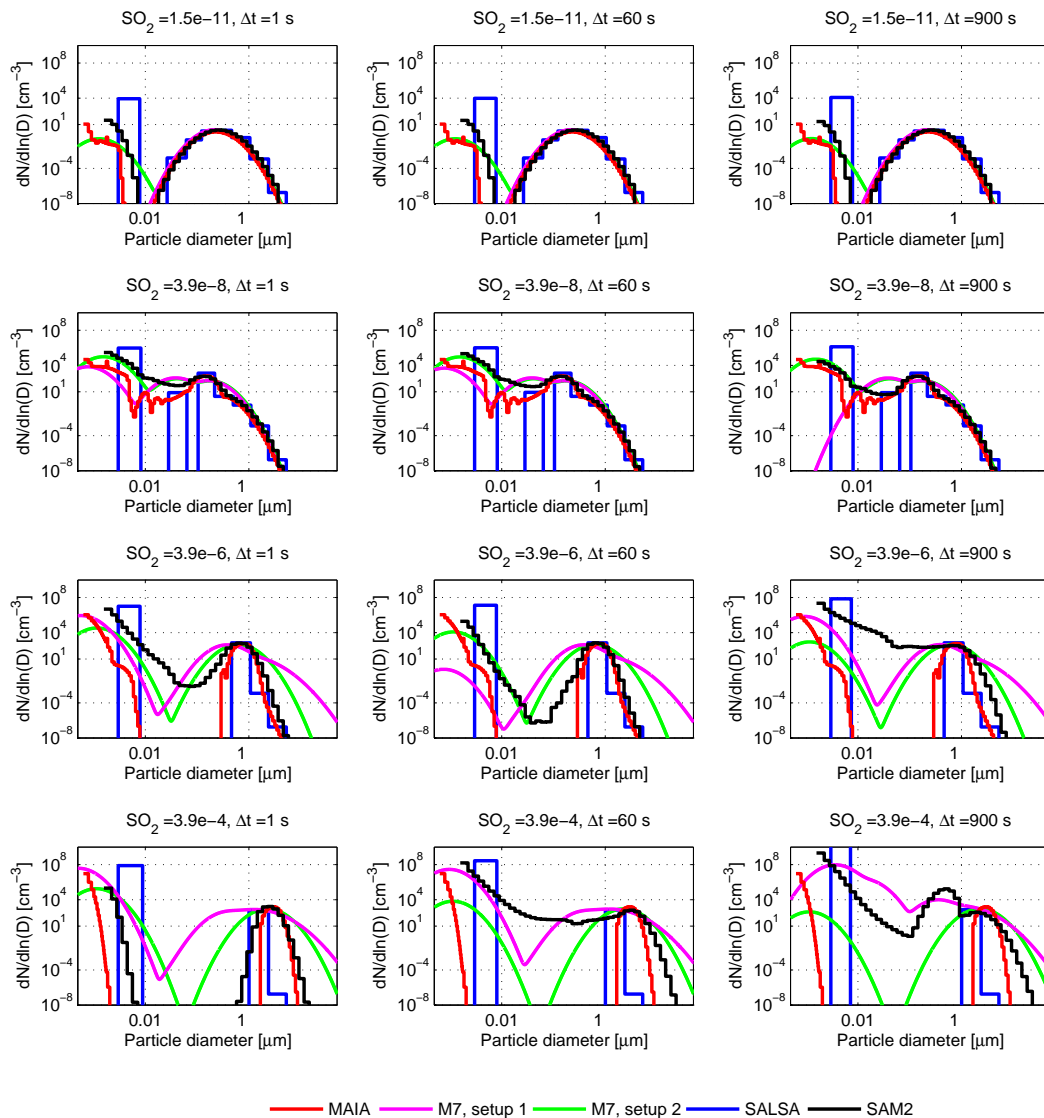


**Fig. 2.** Aerosol number size distributions at noon of the 10th day of the simulations calculated using different aerosol microphysics modules and the reference model. The size distributions were calculated for four different initial gas phase  $\text{SO}_2$  mixing ratios and three different time step lengths  $\Delta t$ . The  $\text{SO}_2$  mixing ratios ( $\text{kg kg}^{-1}$ ) and time step lengths are given on the title of each sub-figure.

- Setup 1, default size distribution of M7;  $\sigma_g=1.59$  for nucleation, Aitken and accumulation mode,  $\sigma_g=2.00$  for coarse mode.
- Setup 2,  $\sigma_g=1.59$  for nucleation, Aitken and accumulation mode, no coarse mode.

## 5 Results and discussion

### 5.1 Size distributions

First, we compared the shapes of aerosol size distributions calculated by individual aerosol microphysics modules when

the size distribution is modified by gas-to-particle conversion of sulphate.

In Fig. 2, the number size distributions at 12:00, 10 days into the simulations are shown for the given different initial gas phase mixing ratios and different time step lengths. Each row in Fig. 2 represents a simulation using a specific initial mixing ratio of  $\text{SO}_2$  and the columns represent the time step length. The mixing ratios and time step lengths are denoted in the title of each subplot.

From Fig. 2, we can see that all microphysics modules reproduce the shape of the size distribution given by the reference model well for background conditions and also when the  $\text{SO}_2$  load was moderately enhanced (two upper rows).



Also in these cases, the time step length has no significant effect on the final size distribution.

As the initial SO<sub>2</sub> mixing ratio is increased, the size distributions begin to differ for the individual microphysics modules (two lowest rows). Increased SO<sub>2</sub> mixing ratios yield to a separation of the aerosol size distributions into two narrow modes in the ultrafine regime of the size spectrum and the coarse mode respectively. The feature is pronounced for the case representing conditions in the stratosphere in the course of a large volcanic eruption (bottom row). Although no direct particle number concentration measurements are known to have been carried out immediately after volcanic eruptions comparable to those considered here in regions where the material was injected into the stratosphere, there is evidence from in situ observations that clearly separated bi-modal particle spectra will evolve under conditions as assumed in this study. Brock et al. (1993) conducted aircraft measurements in the subtropical northern hemisphere, starting 10 weeks after the eruption of Mt. Pinatubo in 1991. During the first days of the campaign particle size spectrometers registered not continuously but in more than 1/3 of all measurements bi-modal size spectra where a distinct and clearly separated coarse mode appeared beyond particles sizes of 1 μm in diameter. Since the flights were carried out in heights below 40 hPa the authors conclude to measure “fallout” from higher elevations. Due to the fact that these spectrometers were calibrated for sulphuric acid only and volcanic ash fallout terminates after a couple days after it was injected into the stratosphere (Guo et al., 2004), it can be assumed that these ultra large particles contain mainly sulphuric acid.

As can be seen from Fig. 2, when the SO<sub>2</sub> mixing ratio is above background levels, M7 with a fixed standard deviation cannot reproduce the shape of the size distribution at the upper end of the spectrum. The sectional approach has advantages to reproduce the narrow band structure of the size distribution in the coarse mode nearly independent on the number of sections used to discretize the aerosol spectrum. Under assumed volcanic conditions the default mode setup of M7 also fails to reproduce the distinct bimodal characteristic of the size distribution in particular when the global model time step length of 900 s is used.

In SALSA, to minimize the amount of tracers, only the number concentration is calculated for the size sections in subregion 3. Also, no coagulation between the particles in subregion 3 is assumed, so these size sections are treated as a sink for smaller particles and condensing gases. In normal atmospheric conditions this assumption is valid, but it fails in the volcanic case. This is more evident in the effective radius as will be shown later in Sect. 5.3.

The sensitivity of the modules to the integration time step length increases as the initial SO<sub>2</sub> mixing ratio increases due to the fact that high concentrations of sulphate yield to rapid changes in aerosol concentrations and particle sizes. For example for  $3.9 \times 10^{-4}$  kg/kg, SAM2 describes extremely well the final size distribution when time step length of 1 s is used,

whereas for Δ*t* of 60 and 900 s a distinctly bimodal distribution does not appear at the end of the simulation. The evolution of the size distributions as predicted by M7 and SALSA is less affected by the integration time increment. When changing the time step length, most notable differences in the size distribution are seen, in particular for M7 setup 1, for particles in the nucleation and accumulation mode.

## 5.2 M7 with different mode setups

As seen in Fig. 2, according to the reference model MAIA, under high concentrations of SO<sub>2</sub> the size distribution is separated in two narrow modes at the end of simulation. These separated modes cannot be reproduced by M7 setups 1 and 2. Therefore, we introduce a third mode setup to get a better agreement for the simulations with high concentrations of SO<sub>2</sub>. The third mode setup is as follows:

- Setup 3,  $\sigma_g=1.59$  for nucleation and Aitken mode,  $\sigma_g=1.2$  for accumulation mode, no coarse mode.

In this section, we investigate the result calculated using M7 with the three different mode setups described above. Figure 3 shows the aerosol number size distributions at 12:00, 10 days into the simulation compared to the results calculated by the reference model MAIA (red curve). Simulations with M7 were done using time step of 900 s. The magenta curves are calculated using the default size distribution of M7 (setup 1), the green curves are for the mode setup 2, and the blue dashed curves are for mode setup 3.

Figure 3a represents simulations for the background concentration of SO<sub>2</sub>. It can be seen that the reference size distribution given by MAIA is well reproduced by the mode setups 1 and 2. This is because the size distribution is only slightly modified by the small concentrations of sulphate produced from SO<sub>2</sub> oxidation. As expected, under these conditions M7 setup 3 with  $\sigma_g=1.2$  for the accumulation mode is not able to reproduce the shape of the size distribution.

In Fig. 3b, the initial SO<sub>2</sub> mixing ratio is set to an intermediate value of  $3.9 \times 10^{-8}$  kg/kg and the processing of the size distribution by sulphuric acid formed in the gas phase becomes more pronounced than in Fig. 3a. In this simulation, MAIA clearly predicts a multi-modal distribution which arises from evolving nucleation bursts through particle growth. MAIA predicts a well-established narrow peak at approximately 0.15 μm on top of the accumulation mode. Even though this peak cannot be reproduced by the M7 setups 1 and 2, their curves follow relatively well the size distribution calculated using the reference model. M7 in setup 3 reproduces best the size distribution for the fine modes, but the number concentration at the upper end of the size spectrum is underestimated.

Figure 3c is a simulation under conditions of an assumed volcanic eruption resulting in mixing ratio of  $3.9 \times 10^{-4}$  kg/kg SO<sub>2</sub>. As seen before, in this simulation, the size distribution is divided into two separate narrow modes of

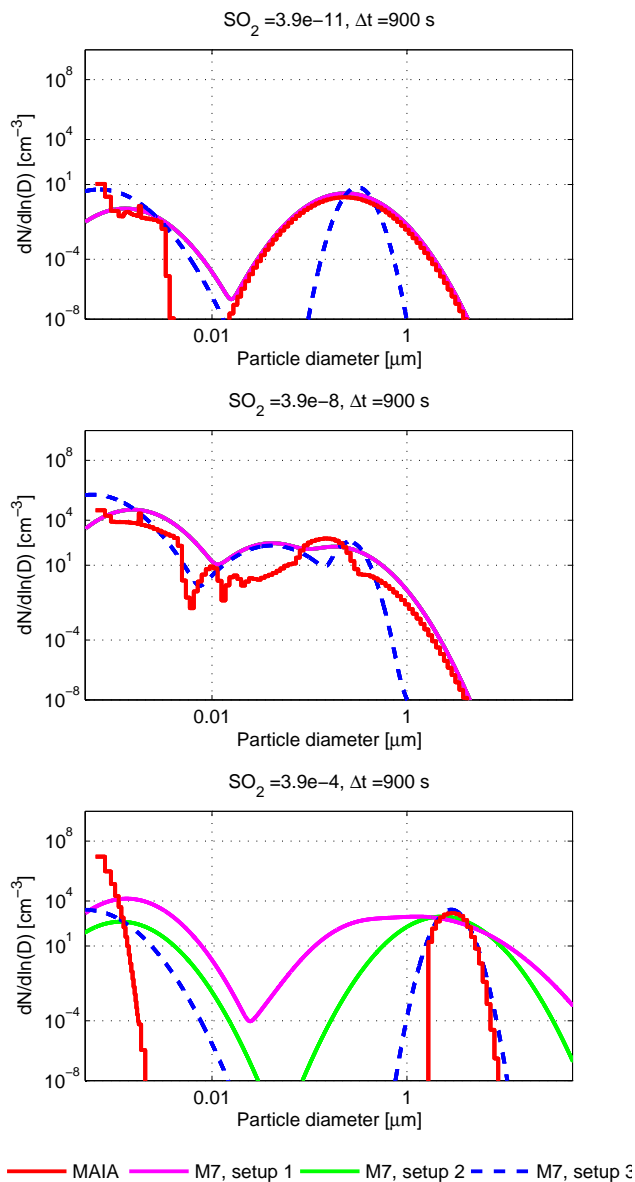


**Fig. 3.** The aerosol number size distribution at noon of the 10th day of the simulation calculated using the reference model MAIA and M7 with three different mode setups for different initial  $\text{SO}_2$  concentrations: (a)  $1.5 \times 10^{-11}$  kg/kg, (b)  $3.9 \times 10^{-8}$  kg/kg, and (c)  $3.9 \times 10^{-4}$  kg/kg.

nucleating particles and coarse particles grown by coagulation and condensation of sulphuric acid.

A distinct coarse mode formed by sulphate particles in the size range between 1 and 10  $\mu\text{m}$  in diameter already one day into the simulation. The predicted standard deviation of such a mode varies in particular depending on the description of the size distribution in the modules, as shown in Fig. 3c.

From Fig. 3c we can see that the default mode setup of M7 (setup 1) overestimates the size distribution at the upper end of the spectrum with a coarse mode  $\sigma_g=2.0$ . Overestimation of large particles in this setup will likely affect the removal of particles in a volcanic plume and potentially has implications in radiative transfer calculations and respective climate responses. With MAIA as reference, M7 in the mode setup 3 gives the best fit for size distributions under assumed high stratospheric concentrations of  $\text{SO}_2$  while the mode setup 2 falls in between the results given by setups 1 and 3.

### 5.3 Effective radius

Since the shape of the aerosol size distribution affects specific aerosol parameters which are relevant to several aerosol-climate interactions (e.g. Dusek et al., 2006), we now discuss the effective radius, a key variable that is used in radiative transfer calculations. The aerosol effective radius is the mean radius of the aerosol size distribution weighted by the aerosol cross sectional area and a measure which part of the wavelength spectrum is mostly affected. Particles with a larger effective radius ( $R_{\text{eff}} > 0.7 \mu\text{m}$ ) absorb more in the near infrared and infrared part of the spectrum than particles with a smaller effective radius, e.g. 0.17  $\mu\text{m}$  (background), which leads to an increase in the aerosol induced radiative heating. Lacis et al. (1992) demonstrated that the climate forcing of stratospheric aerosol can be characterized with the aerosol effective radius. If the effective radius is equal or greater 2  $\mu\text{m}$  the global average greenhouse effect of the aerosol exceeds its albedo effect leading to net surface heating. Also other mean variables for the size of the particle population, such as surface area density or volume area density can be used. Nevertheless, since we have neglected the removal of particles in the model setup, surface area or volume density result are greatly overestimated. Also, for the cases investigated here, the surface area densities and volume densities given by the different modules show qualitatively very similar characteristics as the effective radii. Thus for the sake of clarity, only effective radii are examined here.

Figure 4 is structured as follows: the rows represent the evolution of the effective radii as predicted by the aerosol modules for three different initial  $\text{SO}_2$  mixing ratios, whereas the columns represent the parameter derived from specific integration ranges. In the left column of Fig. 4, the effective radii were derived for the whole size range of particles as treated in the modules. Nevertheless, the effective radius from global model results is often compared to respective data retrieved from optical remote sensing technologies (e.g. satellite instruments, Lidar). With respect to water soluble aerosols, the measurement uncertainties of those retrievals increase exponentially for particles with radius below 0.1  $\mu\text{m}$  (e.g. Dubovik et al., 2000; Thomason et al., 2008). Thus, we believe that the derived parameters of our model simulations are better represented when the integration of the effective radius is adapted for the size range of aerosol

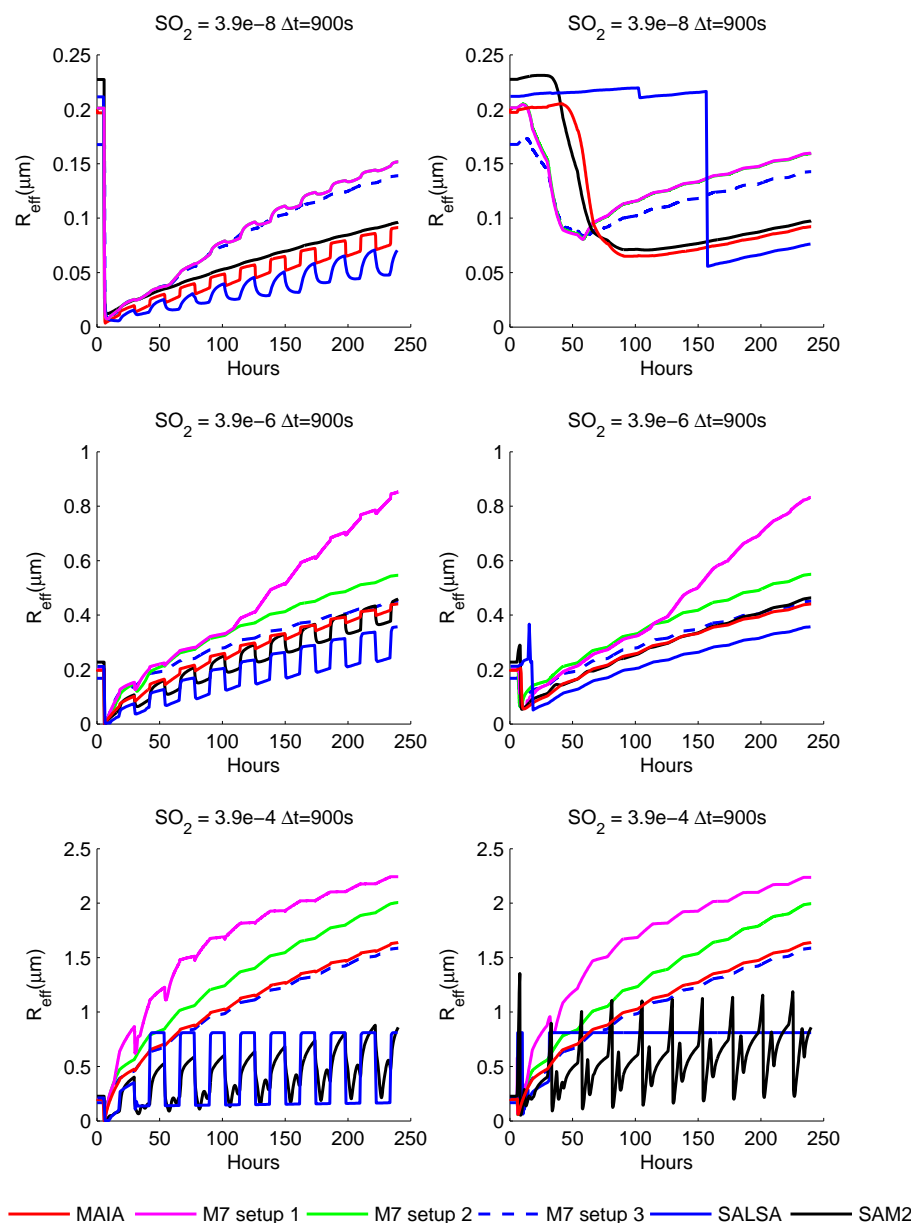


**Fig. 4.** Evolution of the effective radius for the modules MAIA, SALSA, SAM2, and M7 in three mode setups, using three different  $\text{SO}_2$  mixing ratios ( $\text{kg kg}^{-1}$ ). In the left column  $R_{\text{eff}}$  is derived for the whole aerosol size range as defined by the modules, in the right column the integration range starts at  $0.05 \mu\text{m}$ .

particles detectable by remote sensing instruments. Therefore, in the right column of Fig. 4 the model results were filtered to represent the particle size above a threshold size of radius  $R \geq 0.05 \mu\text{m}$ . For all integrations shown in Fig. 4 a time step length of 900 s was used, which is normally applied when the modules are integrated coupled to the global climate model ECHAM5.

The initial mixing ratios shown here range from slightly and moderately increased stratospheric  $\text{SO}_2$  abundances of

$3.9 \times 10^{-8} \text{ kg/kg}$  in the upper row, and  $3.9 \times 10^{-6} \text{ kg/kg}$  in the middle row. The bottom panels show how the effective radii are predicted under assumed volcanic conditions with  $\text{SO}_2 = 3.9 \times 10^{-4} \text{ kg/kg}$ .

### 5.3.1 General behaviour

Before we discuss the module performance for specific  $\text{SO}_2$  initial concentrations, the general behaviour in predicting the effective radius shall be analyzed. Although in Fig. 2 the

aerosol number distributions given by the different aerosol modules appear very similar at moderately increased stratospheric  $\text{SO}_2$  concentrations, Fig. 4 reveals significant relative differences in the evolution of the effective radii given by the different modules. Under all conditions a rapid change appears in the evolution of the effective radius in the very first model time steps.

Excluding the highest  $\text{SO}_2$  concentration case, all modules rapidly drift towards a more or less similar state and predict size distributions whose effective radii are smaller by a factor of 2 to 3 than those of the respective initial size distributions, which we assume to represent a typical stratospheric background state in which ultrafine particles were not considered. This drop in  $R_{\text{eff}}$  results from the formation of particles in the nucleation size range, which are a consequence of  $\text{SO}_2$  oxidation when we prescribe the availability of OH during daylight after 6 h of simulation. After dropping to a certain value, the effective radii increase due to further mass transfer of sulphur from the gas to the particle phase which evolve the aerosol distributions towards the coarse mode. The aerosol mass in the modules constantly increases since we neglect the non-microphysical particle sink terms in this experiments. During night, when new particle formation is inhibited, the effective radii increase sharply due to the absence of a nucleation burst and the rapid growing of ultrafine particles. Then further condensation of  $\text{H}_2\text{SO}_4$  constantly depletes its gas phase reservoir and the mass transfer rate is smaller during night than during day when the availability of OH leads to gaseous sulphuric acid production. Consequently, changes in  $R_{\text{eff}}$  are smaller during night.

Our investigations revealed that the magnitude of the diurnal cycle in  $R_{\text{eff}}$  is related to the shape of the modeled size distribution and depends on module specific definitions. Assuming that MAIA tends to represent the nature of an evolving aerosol effective radius, in the sectional modules SAM2 and SALSA the diurnal cycle in the evolution of  $R_{\text{eff}}$  amplifies when the stratospheric  $\text{SO}_2$  load is increased. In contrast, the modal module M7,  $R_{\text{eff}}$  evolves relatively smoothly. The predicted size distribution in M7 is less affected by fluctuations in the Aitken mode between day and night, because standard deviations  $\sigma_g$  of the individual modes are predefined and cannot vary: In M7 the condensational flux is partitioned over four bands representing the aerosol size distribution (the flux is calculated according to the condensation sink of the individual modes). After the sunset, the nucleation mode particle concentration tends to zero and the available gas is transferred to higher modes only. This yields to a slightly increasing median radius in each mode, not affecting the width of their lognormal distribution. As can be seen from Fig. 2, when initial  $\text{SO}_2$  mixing ratios are increased and a nucleation burst appears during the day, SAM2 shows no distinct bimodal size distribution. During night, aerosols in nucleation sizes are not present and Aitken mode particles grow towards the accumulation mode (not shown). Thus the lowermost range of the predicted size distribution strongly varies

depending on the availability of sunlight (here abstracted by the diurnal cycle in OH concentration). Consequently, in SAM2 the magnitude of the diurnal cycle in  $R_{\text{eff}}$  increases as the mass transfer rate onto the particles increases due to higher  $\text{SO}_2$  mixing ratios. In SALSA, the mechanism to amplify the diurnal cycle in  $R_{\text{eff}}$  is similar to that of SAM2 but the coarse representation of the aerosol size distribution further amplifies the diurnal cycle.

From the right column of Fig. 4 it can be seen that filtering the results in respect of an instruments lower detection limit at  $0.05 \mu\text{m}$ , the predicted effective radii might evolve differently compared to the parameter when derived from the whole size range of the respective module. The differences in the filtered and non-filtered effective radius increase for lower stratospheric  $\text{SO}_2$  concentrations, since the “signal-to-noise ratio” is much weaker than under volcanic conditions. At the end of the simulation, for the lowest  $\text{SO}_2$  concentrations shown in Fig. 4 the difference in  $R_{\text{eff}}$  relative to the parameter derived from the whole size range can reach 15% in the case of SALSA. Furthermore it can be seen that the formation of a diurnal cycle in the evolution of the effective radius is mainly caused by small particles. Whether the predicted size distributions in the nucleation and Aitken mode are affected by diurnal changes or not, it has an almost negligible effect on the filtered effective radii.

From the differences between the filtered and non-filtered values of the effective radius shown in Fig. 4, it can be concluded that subjecting model results to constraints of observational aerosol data, such as detection cut-off size may lead to difficulties in the interpretation of the model results. Knowing and accounting for exact specifications, e.g. detection limits, of respective instruments is essential when predictions of aerosol size distributions are intended for such applications.

### 5.3.2 Low $\text{SO}_2$ concentration

The upper row of Fig. 4 shows the evolution of the effective radii as predicted by the modules, when the initial mixing ratio of stratospheric  $\text{SO}_2$  is  $3.9 \times 10^{-8} \text{ kg kg}^{-1}$ . As shown in Fig. 2, in M7 setup 1, no clear bimodal distribution is predicted for  $\text{SO}_2 = 3.9 \times 10^{-8} \text{ kg/kg}$ , 900 s time step. In this simulation, in M7, particles do not grow to coarse mode size, so the effective radii are equal when mode setups 1 and 2 are used. Also, M7 setup 3 gives qualitatively similar, but slightly lower values for the effective radius. Compared to MAIA, the modal module clearly overestimates the effective radius towards the end of the simulation by  $\sim 90\%$ .

When the effective radius is calculated for the whole size range, SALSA reproduces similar diurnal variation for the effective radius as MAIA, finally underestimating  $R_{\text{eff}}$  of MAIA in the mean by  $\sim 20\%$ . SAM2 predicts very similar values as MAIA for the effective radius during night time, but does not show a significant diurnal cycle, since deviations in the predicted size distribution between day and night

time turn out weaker than in the other modules (not shown in detail). The diurnal variation in  $R_{\text{eff}}$  is increased in SAM2 when the mass flux from the gas to particle phase is getting stronger and particles are predicted to grow faster. This in turn is accompanied by notable differences in the size distribution between day and night, thus amplifying the diurnal variation in  $R_{\text{eff}}$ .

After setting the cut-off size of the effective radii to  $0.05 \mu\text{m}$  (top right panel) and filtering the results, all modules show increasing effective radii in the beginning of the simulation before the effective radii decrease to a value which is approximately twice as high as when the whole particle size range is considered. Owing to its coarse particle size resolution, SALSA predicts a slightly increasing effective radius over about two thirds of the simulation, finally predicting a  $\sim 15\%$  higher  $R_{\text{eff}}$  as when derived from the whole modules size range. In addition, a finer resolution of the aerosol size range seems to better represent the effective radius using the sectional approach, since SAM2 follows most accurately the shape of its evolution as given by MAIA, even when the results are adapted to an optical instrument's lower detection limit.

### 5.3.3 Moderate $\text{SO}_2$ concentration

When the initial  $\text{SO}_2$  mixing ratio is increased to  $3.9 \times 10^{-6} \text{ kg/kg}$ , the setups 1 and 2 of M7 overestimate the effective radius for both integration ranges compared to the reference model. Since the aerosol is growing into a narrow mode of large particles as shown in Fig. 2, M7 setup 1 cannot reproduce the width of this mode, hence the effective radius is overestimated. Generally, under the conditions considered here the representation of the effective radius in M7 is improved when no coarse mode is defined. When mode setup 1 is used, as the effective radius exceeds  $0.3 \mu\text{m}$ , particles are transferred in M7 from the accumulation mode to the coarse mode and the effective radius increases more rapidly than when mode setups 2 and 3 are used. Compared to MAIA at the end of the simulation,  $R_{\text{eff}}$  is overestimated by  $\sim 100\%$  in setup 1 and  $\sim 40\%$  in setup 2, while the evolution of  $R_{\text{eff}}$  in setup 3 almost accurately follows that of the reference model with  $\sim 2\%$  relative difference at the end of the simulation.

Relative to the reference model, SAM2 gives good results here as well for the effective radius, with nearly overlapping curves for the filtered parameter. The relative difference between the effective radius given by MAIA and SAM2 is less than  $5\%$  throughout most of the simulation. At the end of the simulation the relative difference is  $\sim 5\%$ . SALSA performs qualitatively as in the case of lower  $\text{SO}_2$  concentrations, but when the whole size range is considered in retrieving  $R_{\text{eff}}$ , the diurnal cycle is pronounced. At the end of the simulation, the relative difference in predicting  $R_{\text{eff}}$  compared to MAIA slightly increases to approximately  $27\%$  (mean of the last days diurnal cycle).

### 5.3.4 High $\text{SO}_2$ concentration

In the conditions chosen here to represent the stratosphere after an injection of  $\text{SO}_2$  from a large Mt. Pinatubo scale tropical volcanic eruption, the differences between the modules become distinct. When the global model time step length is used, the modules SALSA and SAM2 seem not be able to reproduce an effective radius as observed in the first month after e.g. the Mt. Pinatubo eruption in early summer 1991 (Russell et al., 1996; WMO/SPARC, 2006).

As shown in Fig. 2, the high concentration of gaseous sulphuric acid produced by  $\text{SO}_2$  oxidation leads to the formation of a mode of large particles. The median radius of the mode is approximately an order of magnitude larger than the median radius of the large particle mode which appears under background conditions. During the first two days in the simulation, in M7 setup 1 the aerosols grow rapidly into the coarse mode with  $\sigma_g=2.0$ , causing a general overestimation of the effective radius compared to the reference model MAIA ( $\sim 40\%$  at the end of simulation). With  $\sim 25\%$  for M7 setup 2 the overestimation is lower but significant, because as seen earlier in Sect. 5.2, M7 setup 2 better represents the very narrow mode of large particles as predicted by MAIA. Changing the standard deviation of the accumulation mode in M7 setup 3 to  $\sigma_g=1.2$  and neglecting the coarse mode leads to a much improved agreement of  $R_{\text{eff}}$  compared to MAIA. The relative difference at the end of the simulation is  $\sim 2\%$ .

The coarse resolution of SALSA causes an inaccuracy in the calculated effective radius even though the shape of the size distribution matches well with the size distribution of MAIA (Fig. 2). To reduce the amount of tracer variables, for the three largest size sections in SALSA only the number concentration and the fixed mean radius of the size section are stored, so condensation and coagulation can not increase the size of these particles. Only the growth of particles from smaller subregions affects the number concentration and the largest size classes (see Kokkola et al., 2008). In Fig. 4 it can be seen that this assumption of fixed size sections in subregion 3 is not favorable under extreme volcanic conditions as the effective radius of particles larger than  $0.05 \mu\text{m}$  reaches a constant value.

For the assumed volcanic perturbation of the stratosphere, SAM2 fails to represent the evolution of the effective radius. Since in this aerosol module particle growth due to condensation of  $\text{H}_2\text{SO}_4$  is treated as an advective type process explicitly in time (see Sect. 2.4), the applied CFL criterion (e.g. Jacobson, 2005) limits the total uptake of sulphuric acid vapour through a limitation of the particles growth rate (particles are not allowed to grow beyond the size of their neighboring size section). This also means that the integration time step length and the width of the aerosol size sections as chosen in the module setup ultimately determine a threshold saturation on which such a mass transfer limitation begins to exert. Here, in the assumed volcanic case, condensational growth is strongly underestimated in SAM2, leading to an asymptotic

evolution of  $R_{\text{eff}}$ . This limitation of the  $\text{H}_2\text{SO}_4$  mass flux onto the particles also accounts for the amplification in the diurnal cycle in the evolution of the effective radius as well as for the formation of lower order oscillations preceding the night time increase in  $R_{\text{eff}}$ .

## 6 Conclusions

We have conducted an intercomparison of aerosol microphysics modules for use in the climate model ECHAM5. We studied the evolution of an aerosol size distribution in an environment assumed to be representative in the stratosphere after the injection of  $\text{SO}_2$  from modest to Mt. Pinatubo scale volcanic eruption.

It was found that the time increment used in the module integration can affect the predicted shape of the aerosol distribution. These differences are emphasized with increasing  $\text{SO}_2$  mixing ratios. Whereas the definition of the mode structure in modal modules mainly account for this distinct different model behaviour, it is thought that in sectional modules these differences are caused by the representation of aerosol-microphysical parameterisations.

To further improve the ability of the modules to be used in global model studies of the climate impact from large volcanic eruptions, we have presented a new method for the integration of the time evolution equation for gas phase  $\text{H}_2\text{SO}_4$  to be used in the ECHAM5-HAM microphysics module M7. The new time integration method outperforms the original M7 scheme as well as the Euler backward method when using the ordinary differential equation solver VODE as a reference. In M7 the fixed standard deviation was shown to be problematic when the size distribution is heavily modified by high concentrations of gaseous sulphuric acid. Then the assumption of  $\sigma_g=2$  for the coarse mode results in a “tail” of too large particles. This “tail” causes an overestimation of the effective radius of the coarse mode increasing the estimated sedimentation velocity of the particles and can lead to an unrealistically reduced lifetime of stratospheric sulphate aerosols depending on how sedimentation is treated. Also, a too broad coarse mode might also lead to an overestimation of the radiative response of a large volcanic eruption before the coarse particles are sedimented. This finding is extremely important for stratospheric aerosol modeling, because stratospheric sulphate particles are not deposited as quickly as in the troposphere and their lifetime is much longer.

A more general solution than the simple changing of the distribution  $\sigma_g$  of the log-normal distribution could be the development methods for alternating the standard deviation in different modes. This would nevertheless increase the number of prognostic variables, hence it degrades M7’s computational benefits. The numerical treatment of competing aerosol microphysical processes becomes important under high concentrations of  $\text{SO}_2$  when the mass flux onto the particles is highest. Then other techniques than “classical” op-

erator splitting and the explicit treatment of condensational growth can be favoured as seen from improving the performance of the module M7 or even from the reference model MAIA.

*Acknowledgements.* The work contributed to the Super Volcano project at the Max-Planck Institute for Meteorology. H. Kokkola is supported by the Academy of Finland (project 119471). C. Timmerck is supported by the German Science Foundation DFG grant TI 344/1-1. J. Kazil is supported by the EC project EUCAARI. R. Hommel and U. Niemeier are partially supported by the EC project SCOUT-O3. We would also like to thank Stefan Kinne for his helpful comments and Hanna Vehkamäki for providing an updated version of her nucleation parameterization.

Edited by: V. Grewe

The service charges for this open access publication have been covered by the Max Planck Society.

## References

- Adams, P. J. and Seinfeld, J. H.: Predicting global aerosol size distributions in general circulation models, *Journal of Geophysical Research (Atmospheres)*, 107, 4–1, doi:10.1029/2001JD001010, 2002.
- Brock, C., Jonsson, H., Wilson, J., Dye, J., Baumgardner, D., Borrmann, S., Pitts, M., Osborn, M., DeCoursey, R., and Woods, D.: Relationships between optical extinction, backscatter and aerosol surface and volume in the stratosphere following the eruption of Mt. Pinatubo, *Geophys. Res. Lett.*, 22, 2555–2558, 1993.
- Brown, P. N., Byrne, G. D., and Hindmarsh, A. C.: VODE, A Variable-Coefficient ODE Solver, *SIAM J. Sci. Stat. Comput.*, 10, 1038–1051, 1989.
- Chen, Y. and Penner, J. E.: Uncertainty analysis for estimates of the first indirect aerosol effect, *Atmos. Chem. Phys.*, 5, 2935–2948, 2005, <http://www.atmos-chem-phys.net/5/2935/2005/>.
- Chlond, A.: Locally modified version of Bott’s advection scheme, *Mon. Weather Rev.*, 122, 111–125, 1994.
- Clegg, S. L., Rard, J. A., and Pitzer, K. S.: Thermodynamic properties of 0–6 mol kg<sup>-1</sup> aqueous sulfuric acid from 273.15 to 328.15 K, *J. Chem. Soc., Faraday Trans.*, 90, 1875–1894, doi:10.1039/FT9949001875, 1994.
- Crutzen, P. J.: Albedo Enhancement by Stratospheric Sulfur Injections: A Contribution to Resolve a Policy Dilemma?, *Clim. Change*, 77, 211–220, doi:10.1007/s10584-006-9101-y, <http://www.springerlink.com/content/t1vn75m458373h63>, 2006.
- Curtius, J., Froyd, K. D., and Lovejoy, E. R.: Cluster ion thermal decomposition (I): Experimental kinetics study and ab initio calculations for  $\text{HSO}_4^- (\text{H}_2\text{SO}_4)_{(x)} (\text{HNO}_3)_{(y)}$ , *J. Phys. Chem. A.*, 105, 10867–10873, 2001.
- Dubovik, O., Smirnov, A., Holben, B. N., King, M. D., Kaufman, Y. J., Eck, T. F., and Slutsker, I.: Accuracy assessments of aerosol optical properties retrieved from Aerosol Robotic Network (AERONET) Sun and sky radiance measurements, *J. Geophys. Res.*, 105(D8), 9791–9806, 2000.
- Dusek, U., Frank, G. P., Hildebrandt, L., Curtius, J., Schneider, J., Walter, S., Chand, D., Drewnick, F., Hings, S., Jung, D.,

- Borrmann, S., and Andreae, M. O.: Size Matters More Than Chemistry for Cloud-Nucleating Ability of Aerosol Particles, *Science*, 312, 1375–1378, doi:10.1126/science.1125261, <http://www.sciencemag.org/cgi/content/abstract/312/5778/1375>, 2006.
- Fleming, J. R.: *Historical Perspectives on Climate Change*, Oxford University Press, New York, 1998.
- Froyd, K. D. and Lovejoy, E. R.: Experimental Thermodynamics of Cluster Ions Composed of H<sub>2</sub>SO<sub>4</sub> and H<sub>2</sub>O. 1. Positive Ions, *J. Phys. Chem. A*, 107, 9800–9811, 2003a.
- Froyd, K. D. and Lovejoy, E. R.: Experimental Thermodynamics of Cluster Ions Composed of H<sub>2</sub>SO<sub>4</sub> and H<sub>2</sub>O. 2. Measurements and ab Initio Structures of Negative Ions, *J. Phys. Chem. A*, 107, 9812–9824, 2003b.
- Fuchs, N. A.: *The Mechanics of Aerosols*, Macmillan, 1964.
- Gelbard, F., Tambour, Y., and Seinfeld, J. H.: Sectional representations for simulating aerosol dynamics, *J. Colloid Interface Sci.*, 76, 541–556, 1980.
- Ghan, S., Laulainen, N., Easter, R., Wagener, R., Nemesure, S., Chapman, E., Zhang, Y., and Leung, R.: Evaluation of aerosol direct radiative forcing in MIRAGE, *J. Geophys. Res.*, 106(D6), 5295–5316, 2001.
- Ghan, S. J. and Schwartz, S. E.: Aerosol properties and processes: A path from field and laboratory measurements to global climate models, *Bull. Am. Meteor. Soc.*, 88(7), 1059–1083, doi:10.1175/BAMS-88-7-1059, 2007.
- Giauque, W. F., Hornung, E. W., Kunzler, J. E., and Rubin, T. T.: The thermodynamic properties of aqueous sulfuric acid solutions and hydrates from 15 to 300 K, *Am. Chem. Soc. J.*, 82, 62–70, 1960.
- Guo, S., Rose, W. I., Bluth, G. J. S., and Watson, I. M.: Particles in the great Pinatubo volcanic cloud of June 1991: The role of ice, *Geochemistry, Geophysics, Geosystems*, 5, Q05003, doi:10.1029/2003GC000655, 2004.
- Hamill, P., Toon, O. B., and Kiang, C. S.: Microphysical processes affecting stratospheric aerosol particles, *J. Atmos. Sci.*, 34, 1104–1119, 1977.
- Hanson, D. R. and Lovejoy, E. R.: Measurement of the thermodynamics of the hydrated dimer and trimer of sulfuric acid, *J. Phys. Chem. A*, 110, 9525–9528, doi:10.1021/jp062844w, 2006.
- Herzog M., Weisenstein, D. K., and Penner, J. E.: A dynamic aerosol module for global chemical transport models: Model description, *J. Geophys. Res.*, 109, D18202, doi:10.1029/2003JD004405, 2004.
- Hommel, R.: *Die Variabilität von stratosphärischem Hintergrund-Aerosol. Eine Untersuchung mit dem globalen sektionalen Aerosolmodell MAECHAM5-SAM2.*, Ph.D. thesis, Universität Hamburg, 2008.
- IPCC: *Climate Change 2007: The scientific basis. Contribution of working group I to the fourth assessment report of the Intergovernmental Panel on Climate Change*, Cambridge University Press, New York, 2007.
- Jacobson, M. Z.: *Developing, coupling and applying a gas, aerosol, transport and radiation model to study urban and regional air pollution*, Ph.D. thesis, Dept. of Atmospheric Sciences, University of California, Los Angeles, 1994.
- Jacobson, M. Z.: GATOR-GCMM: A global- through urban-scale air pollution and weather forecast model. 1. Model design and treatment of subgrid soil, vegetation, roads, rooftops, water, sea ice, and snow, *J. Geophys. Res.*, 106(D6), 5385–5402, 2001.
- Jacobson, M. Z.: *Fundamentals of Atmospheric Modeling*, Second Edition, Cambridge University Press, New York, 2005.
- Kazil, J. and Lovejoy, E. R.: A semi-analytical method for calculating rates of new sulfate aerosol formation from the gas phase, *Atmos. Chem. Phys.*, 7, 3447–3459, 2007, <http://www.atmos-chem-phys.net/7/3447/2007/>.
- Kazil, J., Lovejoy, E. R., Jensen, E. J., and Hanson, D. R.: Is aerosol formation in cirrus clouds possible?, *Atmos. Chem. Phys.*, 7, 1407–1413, 2007, <http://www.atmos-chem-phys.net/7/1407/2007/>.
- Kerminen, V. M. and Kulmala, M.: Analytical formulae connecting the “real” and the “apparent” nucleation rate and the nuclei number concentration for atmospheric nucleation events, *J. Aerosol Science*, 33, 609–622, 2002.
- Kokkola, H., Korhonen, H., Lehtinen, K. E. J., Makkonen, R., Asmi, A., Järvenoja, S., Anttila, T., Partanen, A.-I., Kulmala, M., Järvinen, H., Laaksonen, A., and Kerminen, V.-M.: SALSA - a Sectional Aerosol module for Large Scale Applications, *Atmos. Chem. Phys.*, 8, 2469–2483, 2008, <http://www.atmos-chem-phys.net/8/2469/2008/>.
- Lacis, A., Hansen J., and Sato M.: Climate forcing by stratospheric aerosols, *Geophys. Res. Lett.*, 19(15), 1607–1610, 1992.
- Lauer, A., Hendricks, J., Ackermann, I., Schell, B., Hass, H., and Metzger, S.: Simulating aerosol microphysics with the ECHAM/MADE GCM - Part I: Model description and comparison with observations, *Atmos. Chem. Phys.*, 5, 3251–3276, 2005, <http://www.atmos-chem-phys.net/5/3251/2005/>.
- Le Treut, H., Somerville, R., Cubasch, U., Ding, Y., Mauritzen, C., Mokssit, A., Peterson, T., and Prather, M.: *Climate Change 2007: The Physical Science Basis. Contribution of Working Group I to the Fourth Assessment Report of the Intergovernmental Panel on Climate Change*, edited by: Solomon, S., Qin, D., Manning, M., Chen, Z., Marquis, M., Averyt, K. B., Tignor, M., and Miller, H. L., chap. Historical Overview of Climate Change, Cambridge University Press, Cambridge, United Kingdom and New York, NY, USA, 2007.
- Liao, H. and Seinfeld, J.: Global impacts of gas-phase chemistry-aerosol interactions on direct radiative forcing by anthropogenic aerosols and ozone, *J. Geophys. Res.*, 110, D18208, doi:10.1029/2005JD005907, 2005.
- Liu, H. Q., Pinker, R. T., and Holben, B. N.: A global view of aerosols from merged transport models, satellite, and ground observations, *J. Geophys. Res.*, 110, D10S15, doi:10.1029/2004JD004695, 2005.
- Lovejoy, E. R. and Curtius, J.: Cluster ion thermal decomposition (II): Master equation modeling in the low pressure limit and fall-off regions. Bond energies for HSO<sub>4</sub><sup>-</sup> (H<sub>2</sub>SO<sub>4</sub>)<sub>x</sub>(HNO<sub>3</sub>)<sub>y</sub>, *J. Phys. Chem. A*, 105, 10874–10883, 2001.
- Lovejoy, E. R., Curtius, J., and Froyd, K. D.: Atmospheric ion-induced nucleation of sulfuric acid and water, *J. Geophys. Res.*, 109, D08204, doi:10.1029/2003JD004460, 2004.
- McCormick, M. P., Thomason, L. W. and Trepte C. R., Atmospheric effects of the Mt. Pinatubo eruption, *Nature*, 373, 399–404, 1995.
- Rasch, P. J., Crutzen, P. J., and Coleman, D. B.: Exploring the geoengineering of climate using stratospheric sulfate aerosols: The role of particle size, *Geophys. Res. Lett.*, 35, 2809, doi:10.1029/2007GL032179, 2008.
- Niemeier, U., Timmreck, C., Graf, H.-F., Kinne, S., Rast, S., and Self, S.: Initial fate of fine ash and sulfur from large volcanic

- eruptions, *Atmos. Chem. Phys. Discuss.*, submitted, 2009.
- Rasch, P. J., Tilmes, S., Turco, R. P., Robock, A., Oman, L., Chen, C.-C., Stenchikov, G. L., and Garcia, R. R.: An overview of geo-engineering of climate using stratospheric sulfate aerosols, *Phil. Trans. Royal Soc. A*, 366, 4007–4037, doi:10.1098/rsta.2008.0131, 2008.
- Read, W. G., Froidevaux, L., and Waters, J. W.: Microwave limb sounder measurement of stratospheric SO<sub>2</sub> from the Mount Pinatubo volcano, *Geophys. Res. Lett.*, 20, 1299–1302, 1993.
- Reddy, M. S., Boucher, O., Bellouin, N., Schulz, M., Balkanski, Y., Dufresne, J. L., and Pham, M.: Estimates of global multicomponent aerosol optical depth and direct radiative perturbation in the Laboratoire de Meteorologie Dynamique general circulation model, *J. Geophys. Res.*, 110, D10S16, doi:10.1029/2004JD004757, 2005.
- Rodriguez, M. and Dabdub, D. J.: IMAGES-SCAPE2: A modeling study of size and chemically resolved aerosol thermodynamics in a global chemical transport model, *J. Geophys. Res.*, 109, D02203, doi:10.1029/2003JD003639, 2004.
- Roeckner, E., Bäuml, G., Bonaventura, L., Brokopf, R., Esch, M., Giorgetta, M., Hagemann, S., Kirchner, I., Kornbluh, L., Manzini, E., Rhodin, A., Schlese, U., Schulzweida, U., and Tompkins, A.: The atmospheric general circulation model ECHAM5. PART I: Model description, *MPI-Report*, 349, 127 pp., 2003.
- Russell, P. B., Livingston, J. M., Pueschel, R. F., Bauman, J. J., Pollack, J. B., Brooks, S. L., Hamill, P., Thomason, L. W., Stowe, L. L., Deshler, T., Dutton, E. G., and Bergstrom, R. W.: Global to microscale evolution of the Pinatubo volcanic aerosol, derived from diverse measurements and analyses, *J. Geophys. Res.*, 101(D13), 18745–18763, 1996.
- Schneider, D. J., Rose, W. I., Coke, L. R., Bluth, G. J. S., Sprod, I. E., and Krueger, A. J.: Early evolution of a stratospheric volcanic eruption cloud as observed with TOMS and AVI-IRR, *J. Geophys. Res.*, 104(D4), 4037–4050, 1998.
- Seinfeld, J. H. and Pandis, S. N.: *Atmospheric Chemistry and Physics*, John Wiley & Sons inc., 1998.
- Spalding, D. B.: A novel finite-difference formulation for differential expressions involving both first and second derivatives, *Int. J. Num. Methods*, 4, 551–559, 1972.
- Spracklen, D. V., Springle, K. S., Carslaw, K. S., Chipperfield, M. P., and Mann, G. W.: A global off-line model of size-resolved aerosol microphysics, *Atmos. Chem. Phys.*, 5, 3233–3250, 2005, <http://www.atmos-chem-phys.net/5/3233/2005/>.
- Stier, P., Feichter, J., Kinne, S., Kloster, S., Vignati, E., Wilson, J., Ganzeveld, L., Tegen, I., Werner, M., Balkanski, Y., Schulz, M., Boucher, O., Minikin, A., and Petzold, A.: The aerosol-climate model ECHAM5-HAM, *Atmos. Chem. Phys.*, 5, 1125–1156, 2005, <http://www.atmos-chem-phys.net/5/1125/2005/>.
- Thomason, L. W., Burton, S. P., Luo, B.-P., and Peter, T.: SAGE II measurements of stratospheric aerosol properties at non-volcanic levels, *Atmos. Chem. Phys.*, 8, 983–995, 2008, <http://www.atmos-chem-phys.net/8/983/2008/>.
- Timmreck, C.: Three-dimensional simulation of stratospheric background aerosol: First results of a multiannual GCM simulation, *J. Geophys. Res.*, 106(D22), 28313–28332, 2001.
- Timmreck, C. and Graf, H.-F.: A microphysical model to simulate the development of stratospheric aerosol in a GCM, *Meteorol. Zeitschr.*, 9, 263–282, 2000.
- Timmreck, C., Graf, H.-F., and Steil, B.: Aerosol chemistry interactions after the Mt. Pinatubo eruption, 139, 214–225, *AGU Monograph*, 2003.
- Twomey, S.: Pollution and the planetary albedo, *Atmos. Environ.*, 8, 1251–1256, 1974.
- Vehkamäki, H., Kulmala, M., Napari, I., Lehtinen, K. E. J., Timmreck, C., Noppel, M., and Laaksonen, A.: An improved parameterization for sulfuric acid-water nucleation rates for tropospheric and stratospheric conditions, *J. Geophys. Res.*, 107(D22), AAC3.1–AAC3.10, doi:10.1029/2002JD002184, 2002.
- Vignati, E., Wilson, J., and Stier, P.: M7: An efficient size-resolved aerosol microphysics module for large-scale aerosol transport models, *J. Geophys. Res.*, 109, D22202, doi:10.1029/2003JD004485, 2004.
- Weart, S.: *The Discovery of Global Warming*, Harvard University Press, Cambridge, MA, 2003.
- Weisenstein, D. K., Yue, G. K., Ko, M. K. W., Sze, N. D., Rodriguez, J. M., and Scott, C. J.: Atwo-dimensional model of sulfur species and aerosol, *J. Geophys. Res.*, 102(D11), 13019–13035, 1997.
- Weisenstein, D. K., Penner, J. E., Herzog, M., and Liu, X.: Global 2-D intercomparison of sectional and modal aerosol modules, *Atmos. Chem. Phys.*, 7, 2339–2355, 2007, <http://www.atmos-chem-phys.net/7/2339/2007/>.
- Wilson, J. and Raes, F.: M3 a multi modal model for aerosol dynamics, *Proceedings of the 14th International Conference on Nucleation and Atmospheric Aerosols*, 458–461, 1996.
- Wilson, J., Cuvelier, C., and Raes, F.: A modeling study of global mixed aerosol fields, *J. Geophys. Res.*, 106(D24), 34081–34108, 2001.
- WMO/SPARC: *WMO/SPARC Scientific Assessment of Stratospheric Aerosol Properties (ASAP)*, Tech. rep., 2006.
- Zhang, Y., Easter, R. C., Ghan, S. J., and Abdul-Razzak, H.: Impact of aerosol size representation on modeling aerosol-cloud interactions, *J. Geophys. Res.*, 107(D21), 4558, doi:10.1029/2001JD001549, 2002.